nature structural & molecular biology

HflX is a ribosome-splitting factor rescuing stalled ribosomes under stress conditions

Yanqing Zhang[1], Chandra Sekhar Mandava[2], Wei Cao[1], Xiaojing Li[3], Dejiu Zhang[4], Ningning Li[1], Yixiao Zhang[1], Xiaoxiao Zhang[1], Yan Qin[4], Kaixia Mi[3], Jianlin Lei[1], Suparna Sanyal[2] & Ning Gao[1]

Adverse cellular conditions often lead to nonproductive translational stalling and arrest of ribosomes on mRNAs. Here, we used fast kinetics and cryo-EM to characterize *Escherichia coli* HflX, a GTPase with unknown function. Our data reveal that HflX is a heat shock–induced ribosome-splitting factor capable of dissociating vacant as well as mRNA-associated ribosomes with deacylated tRNA in the peptidyl site. Structural data demonstrate that the N-terminal effector domain of HflX binds to the peptidyl transferase center in a strikingly similar manner as that of the class I release factors and induces dramatic conformational changes in central intersubunit bridges, thus promoting subunit dissociation. Accordingly, loss of HflX results in an increase in stalled ribosomes upon heat shock. These results suggest a primary role of HflX in rescuing translationally arrested ribosomes under stress conditions.

Cells have evolved many stress-response systems to deal with the constantly changing environment. The transcriptional regulation of these defense systems has been well characterized in both prokaryotes and eukaryotes. However, very little is known about how cells respond at the translational level. Heat-shock response (HSR) is one of the most conserved cellular regulatory systems[1–3]. Under heat or other stresses, cells respond by extensive transcriptional reprogramming, through sharply elevated transcription of the genes encoding various heat-shock proteins (HSPs); thus, cells have a high demand for active ribosomes to provide massive and timely production of these proteins.

Heat shock usually poses a major challenge for translation machineries. In general, heat shock induces a global repression of translation activity[4], primarily through downregulation of translation initiation[2,4,5]. Importantly, the ribosome is a central hub for quality control for newly synthesized proteins[6,7] and cotranslational mRNA surveillance[8]. Because the growing nascent polypeptides are highly vulnerable to heat shock and are prone to misfolding and aggregation[9,10], temperature upshift is expected to affect translating ribosomes as well. Indeed, perturbation of proteostasis by heat shock[11] or chaperone inhibitors[12] causes a global pausing of ribosomes at the elongation steps. As a consequence, these elongation-stalled ribosomes might turn into nonproductive or even toxic ribosomal complexes, because translation stalling can induce mRNA cleavage[13,14] and cause abortive translation[15]. Therefore, the cellular translation capacity is substantially compromised upon heat stress, which seems to pose a challenge for timely and massive production of HSPs. How cells initiate selective translation of the HSP mRNAs is not well understood. Although the contribution from altered initiation-factor dependence and the temperature-sensing elements in the 5′ untranslated regions of some HSP mRNAs have been recognized (reviewed in refs. 5,16), it is still not clear how selective translation of such a diverse population of HSP mRNAs is achieved under heat stress. Nevertheless, cells must be able to rescue and recycle stalled ribosomes rapidly so that translation of HSP mRNAs can be initiated in time.

In the present work, to understand the possible mechanism of rescuing of stalled ribosomes during HSR, we characterized the conserved GTPase HflX from *E. coli*. Our biochemical and *in vivo* data indicate that HflX, a ribosome-dependent GTPase[17,18], is an HSP with inherent ribosome-splitting activity. HflX targets the post-termination-like complex (PTL), with a deacylated tRNA in the peptidyl (P) site and an empty aminoacyl (A) site, as well as vacant 70S ribosomes, and efficiently dissociates them into free subunits in an IF3-independent manner. Structural analysis of the 50S–HflX complex suggests that HflX promotes subunit dissociation by disrupting the central intersubunit bridges. Our results therefore portray HflX as an alternative ribosome-recycling factor involved in rescuing stalled ribosomes during HSR and suggest that HflX, in a broad context, constitutes an important component in the functional coupling between cotranslational quality control and stress-induced translation reprogramming.

RESULTS

HflX is an HSP required for cell survival upon heat stress

Although HflX is universally conserved[19], bacterial strains with *hflX* deleted (Δ*hflX*) show no apparent phenotype[20–23]. According to previous microarray data, the transcription level of *hflX* increases upon heat

[1]Ministry of Education Key Laboratory of Protein Sciences, Center for Structural Biology, School of Life Sciences, Tsinghua University, Beijing, China. [2]Department of Cell and Molecular Biology, Uppsala University, Uppsala, Sweden. [3]Key Laboratory of Pathogenic Microbiology and Immunology, Institute of Microbiology, Chinese Academy of Sciences, Beijing, China. [4]Key Laboratory of RNA Biology, Institute of Biophysics, Chinese Academy of Sciences, Beijing, China. Correspondence should be addressed to N.G. (ninggao@tsinghua.edu.cn), S.S. (suparna.sanyal@icm.uu.se) or J.L. (jllei@tsinghua.edu.cn).

Received 12 March; accepted 4 September; published online 12 October 2015; doi:10.1038/nsmb.3103

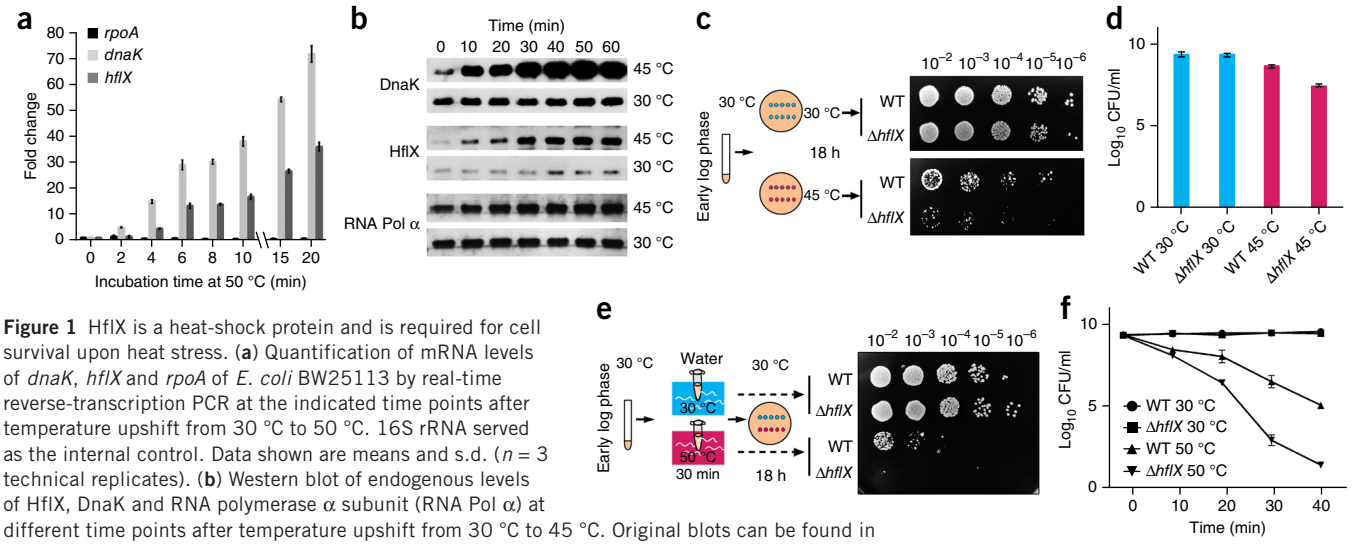

Figure 1 HflX is a heat-shock protein and is required for cell survival upon heat stress. (**a**) Quantification of mRNA levels of *dnaK*, *hflX* and *rpoA* of *E. coli* BW25113 by real-time reverse-transcription PCR at the indicated time points after temperature upshift from 30 °C to 50 °C. 16S rRNA served as the internal control. Data shown are means and s.d. ($n = 3$ technical replicates). (**b**) Western blot of endogenous levels of HflX, DnaK and RNA polymerase α subunit (RNA Pol α) at different time points after temperature upshift from 30 °C to 45 °C. Original blots can be found in **Supplementary Data Set 1**. (**c**–**f**) Spotting assay (**c**,**e**) and determination of CFUs (**d**,**f**). WT (BW25113) and Δ*hflX* (JW4131) strains were exposed to heat stress in two different ways: a long, mild exposure (45 °C, 18 h) in **c** and a short, severe exposure (50 °C, 30 min) in **e**. Spotting assay data in **c** and **e** are representative of three individual experiments. Data in **d** and **f** are means and s.d. ($n = 3$ cell-culture replicates).

shock[24–26]. However, whether HflX is an HSP has not been explicitly examined. To determine this, we first monitored the mRNA level of *hflX* upon temperature upshift to 50 °C. The mRNA level of *hflX* quickly increased upon heat exposure, displaying a similar pattern as that of the typical HSP gene *dnaK* (**Fig. 1a**). In contrast, the level of the constitutively expressed non-HSP gene *rpoA* (encoding the RNA polymerase α subunit) remained relatively constant (**Fig. 1a**). Next, we examined the change in the protein level of HflX upon heat shock at 45 °C. Consistently with the mRNA results, the amount of RNA polymerase α remained unchanged, but we observed a temperature-responsive increase of HflX protein similar to that of HSP DnaK (**Fig. 1b**, **Supplementary Data Set 1** and **Supplementary Note**).

We next sought to determine whether *hflX* is required for cell growth at high temperatures. Whereas wild type (WT) and Δ*hflX* cells showed practically no growth differences at 30 °C, the Δ*hflX* cells grew much more slowly than the WT cells at 45 °C (**Fig. 1c**,**d** and **Supplementary Fig. 1**). According to the values of calculated colony-forming units (CFUs), the presence of HflX in the WT cells conferred 10- to 20-fold greater protection from heat stress than that in the knockout cells (**Fig. 1d**). To further validate whether HflX is involved in protecting cells from thermal killing, we exposed the WT and Δ*hflX* cells to 50 °C for 30 min, a condition in which severe heat stress causes considerable thermal killing, and then allowed the cells to recover at 30 °C. The resulting colony count of the Δ*hflX* cells was substantially lower than that of WT cells (**Fig. 1e**). After a 30-min exposure at 50 °C, the survival rate of the WT cells was about three to four orders of magnitude higher than the that of Δ*hflX* cells (**Fig. 1f**). Together, these results demonstrate that *hflX* is indeed a bona fide heat-shock gene, and HflX is required for protection of the cell from heat stress.

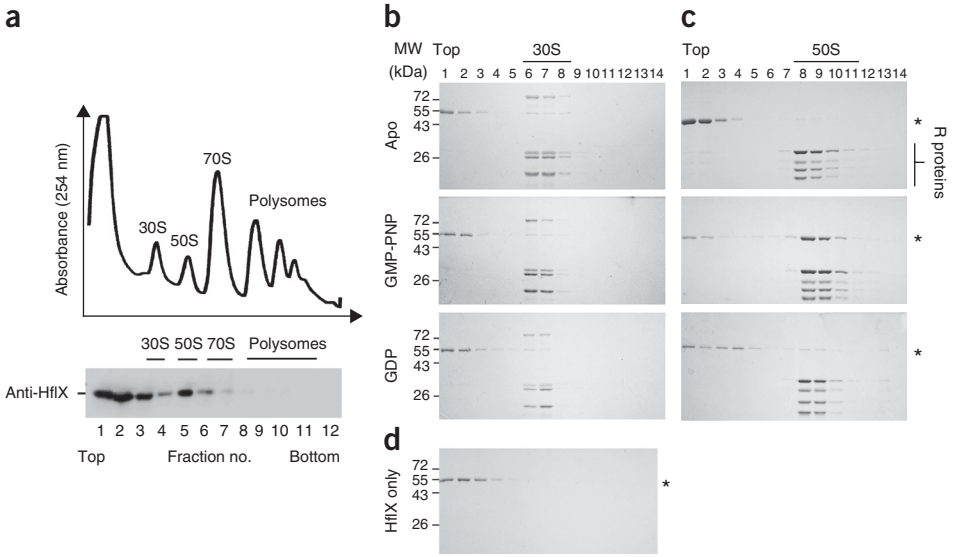

Figure 2 HflX binds to the ribosome *in vivo* and *in vitro*, with a preference for the 50S subunit. (**a**) Endogenous HflX distribution in ribosome fractions examined by polysome profile and western blot analysis. (**b**,**c**) Binding of HflX (three-fold excess) to highly purified 30S (**b**) and 50S (**c**) subunits (0.6 μM), examined by sucrose density gradient centrifugation and SDS-PAGE. MW, molecular weight. (**d**) As in **b** only and **c**, but with HflX. Bands of HflX are indicated by asterisks.

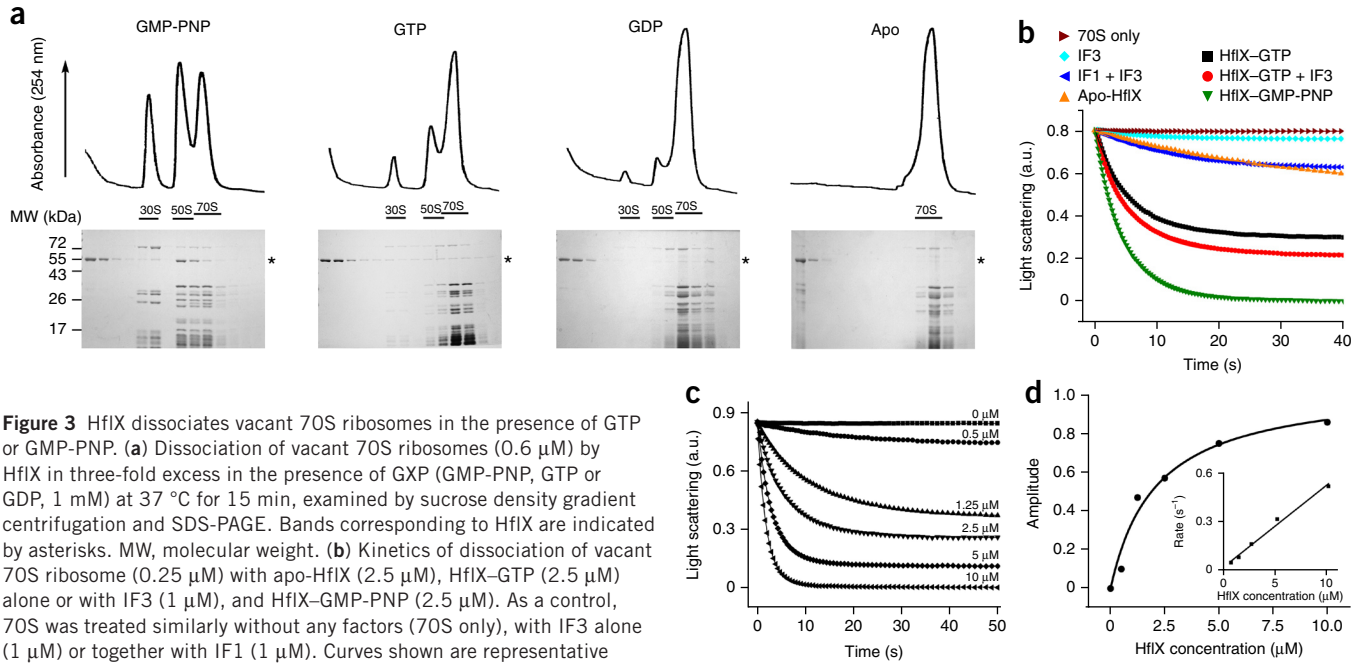

Figure 3 HflX dissociates vacant 70S ribosomes in the presence of GTP or GMP-PNP. (**a**) Dissociation of vacant 70S ribosomes (0.6 μM) by HflX in three-fold excess in the presence of GXP (GMP-PNP, GTP or GDP, 1 mM) at 37 °C for 15 min, examined by sucrose density gradient centrifugation and SDS-PAGE. Bands corresponding to HflX are indicated by asterisks. MW, molecular weight. (**b**) Kinetics of dissociation of vacant 70S ribosome (0.25 μM) with apo-HflX (2.5 μM), HflX–GTP (2.5 μM) alone or with IF3 (1 μM), and HflX–GMP-PNP (2.5 μM). As a control, 70S was treated similarly without any factors (70S only), with IF3 alone (1 μM) or together with IF1 (1 μM). Curves shown are representative of five individual experiments. A.u., arbitrary units. (**c**) Dissociation of 70S (0.25 μM) with increasing concentrations of HflX–GTP. (**d**) The amplitudes from **c** plotted against the concentration of HflX. Inset, observed rates of vacant 70S dissociation (k_{obs}) from **c**, plotted against the concentration of HflX and fitted with a linear function.

HflX preferentially binds to the 50S subunit

Earlier reports have identified that HflX binds to the ribosome, but the nucleotide-dependent binding modes of HflX to different ribosomal fractions have been controversial[17,27–29]. To clarify this discrepancy, we first examined the endogenous HflX distribution in ribosomal fractions by sucrose density gradient centrifugation (SDGC) coupled with western blotting. We detected HflX in the top fractions together with a clear enrichment in the 50S fractions (**Fig. 2a**), thus suggesting stable and preferential binding of HflX to the 50S subunit. We also observed some binding in the 30S and 70S fractions. Next, we tested the binding of HflX to highly purified 30S and 50S subunits with SDGC (**Fig. 2b–d**). HflX, at three-fold excess, bound very weakly to the 30S subunit, and the nucleotides showed no apparent modulation on its 30S binding (**Fig. 2b**). In contrast, the binding of HflX to the 50S subunit was clearly dependent on nucleotides, and we observed substantially higher binding of HflX in the presence of GMP-PNP (**Fig. 2c**). These results clearly show that HflX binds to the ribosome both *in vivo* and *in vitro* and displays a strong preference for the 50S subunit, especially in the presence of the nonhydrolyzable GTP analog.

HflX dissociates empty 70S ribosomes

We also examined HflX binding to 70S ribosomes by SDGC. A similar nucleotide-dependent binding of HflX to the 70S was clearly observable, in the order GMP-PNP > GTP > GDP (**Fig. 3a**). Interestingly, HflX also promoted dissociation of 70S ribosomes into subunits, especially in the presence of GMP-PNP or GTP (**Fig. 3a**). We detected the highest intensity of HflX binding in the separated 50S subunits with GMP-PNP. When we increased HflX to 20-fold excess, HflX–GMP-PNP converted all 70S ribosomes into subunits (**Supplementary Fig. 2a**). We also obtained similar results in freshly prepared cell lysates (**Supplementary Fig. 2b**). *In vivo* overexpression of HflX caused a compromised growth rate together with a marked accumulation of 50S subunits (**Supplementary Fig. 2c–e**).

Next, we followed the kinetics of ribosome dissociation with HflX in stopped flow, by using light scattering as a tool[30]. Whereas apo-HflX showed moderate splitting activity toward vacant ribosomes ($k_{obs\ apo\text{-}HflX} = 0.03 \pm 0.001\ s^{-1}$ (mean ± s.d., $n = 5$ cell cultures)) (**Fig. 3b**), addition of GTP or GMP-PNP markedly increased the splitting efficiency, with rates $k_{obs\ HflX\text{–}GTP} = 0.2 \pm 0.002\ s^{-1}$ and $k_{obs\ HflX\text{–}GMP\text{-}PNP} = 0.22 \pm 0.003\ s^{-1}$. These rates were three times faster than the rate of subunit dissociation with IF1 and IF3 ($k_{obs\ IF1+IF3} = 0.076 \pm 0.007\ s^{-1}$). Moreover, the splitting mediated by HflX–GTP was more stable (higher amplitude) than with IF1 and IF3. A combination of IF3 and HflX–GTP resulted in a small increase in the amplitude but no effect on the rate of the process. As expected, HflX–GMP-PNP showed the highest splitting.

We further estimated the binding parameters of HflX–GTP to the 70S ribosome by titrating HflX–GTP in the 70S dissociation experiments, which increased both the rate and amplitude of the light-scattering curves (**Fig. 3c**). The amplitudes represent the fraction of 70S ribosomes irreversibly dissociated by saturation binding of HflX–GTP. Plotting of amplitude against HflX–GTP concentration produced a hyperbolic fit, from which we estimated the K_d of HflX–GTP binding to 70S as ~1.5 μM (**Fig. 3d**). The observed rates, however, increased linearly as a function of HflX concentration as in a typical bimolecular association reaction (**Fig. 3d**). The k_{on} and k_{off} estimated from the slope and the intercept of the linear fit of the rates are $0.05 \pm 0.003\ \mu M^{-1}\ s^{-1}$ and $0.05 \pm 0.01\ s^{-1}$ respectively. The K_d value calculated from the ratio of k_{off} and k_{on} is 1.0 μM, in good agreement with the K_d estimated from the amplitudes of the light-scattering curves (**Fig. 3d**). From these equilibrium and kinetic characterizations, it is clear that HflX displays a strong 70S-splitting activity independent of GTP hydrolysis and other translation factors.

HflX promotes the breakdown of puromycin-treated polysomes

We next set out to examine whether HflX could split functional ribosomal complexes with mRNA and tRNA. We incubated fractions of purified 70S and polysomes with HflX in the presence of GMP-PNP or GTP and examined the breakdown of polysomes with SDGC. As expected, we observed a decrease in the 70S peak associated with marked increases in the 30S and 50S peaks. In addition, we also observed a decrease in the

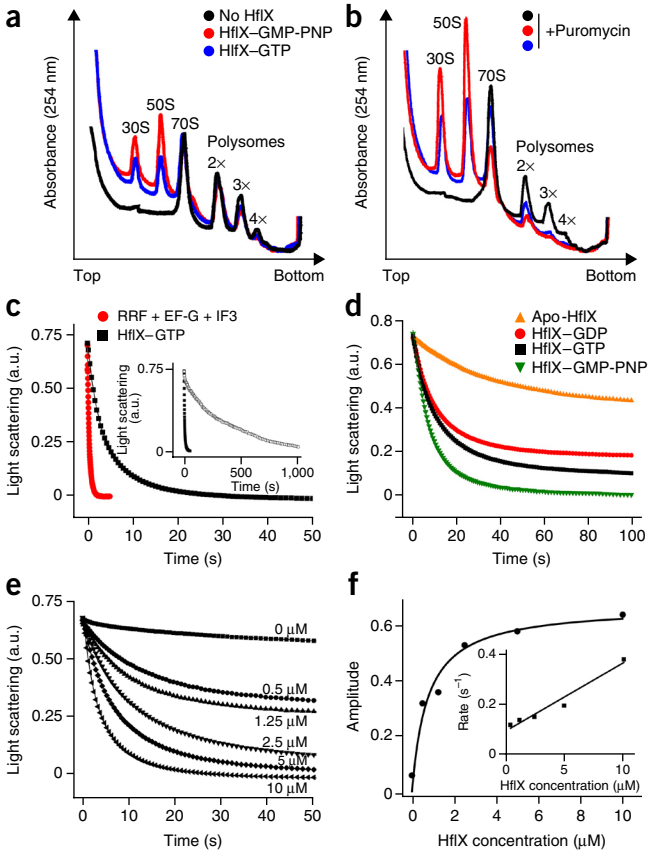

Figure 4 HflX efficiently promotes breakdown of puromycin-treated polysomes and splits the PTL. (**a**) Polysome profile from sucrose density gradient centrifugation of the polysomes (0.1 μM) in the absence or presence of 50-fold excess of HflX with GMP-PNP or GTP. (**b**) As in **a**, but with polysomes (0.1 μM) preincubated with puromycin (0.2 mM). (**c**) Time course of dissociation of mRNA-programmed PTL containing deacylated $tRNA^{Leu}$ in the P site (0.25 μM) with HflX–GTP (10 μM) or with RRF (10 μM), EF-G (5 μM) and IF3 (1 μM). Inset, time course of dissociation of translating ribosome stalled with peptidyl-tRNA ($[^3H]$fMet-Leu-Ile-$tRNA^{Ile}$) in the P site with HflX–GTP (open squares). For visual comparison, data for PTL dissociation are shown (solid squares). A.u., arbitrary units. (**d**) Dissociation of the PTL (0.25 μM) with 2.5 μM each of apo-HflX, HflX–GDP, HflX–GTP or HflX–GMP-PNP. (**e**) Effect of increasing concentration of HflX–GTP on splitting of the PTL (0.25 μM). (**f**) The amplitudes from **e** plotted against the concentration of HflX. Inset, observed rates of dissociation of PTL (k_{obs}) from **e**, plotted against the concentration of HflX and fitted with a linear equation.

polysome levels (70S ribosome, disome, trisome and tetrasome peaks are denoted 1×, 2×, 3× and 4×, respectively), although the breakdown reaction had low efficiency, in the presence of either GTP or GMP-PNP (**Fig. 4a**). The low efficiency of HflX in polysome splitting could be due to the presence of a peptidyl-tRNA at the P site of the polysomic ribosomes. Thus, to change the acylation state of the P-site tRNA, we preincubated polysomes with puromycin—an antibiotic that removes the peptidyl group from the P-site tRNA[31]. HflX markedly decreased the abundance of various forms of puromycin-treated polysomes and caused sharp increases in the abundance of both 30S and 50S subunits (**Fig. 4b**). Thus, these results demonstrate that the splitting activity of HflX depends on the functional state of the ribosome and suggests that the natural substrate of HflX is a ribosomal complex carrying a deacylated tRNA at the P site.

HflX dissociates the PTL

Next, we prepared a PTL with an mRNA-programmed ribosome containing deacylated $tRNA^{Leu}$ in the P site and an empty A site[32], and we studied the kinetics of its dissociation with HflX. This complex mimics a translationally arrested ribosome after peptide release, and it is similar to a post-termination complex, except that a sense codon is present in the A site instead of a stop codon. Similarly to the vacant 70S ribosome, HflX–GTP alone could dissociate the PTL (**Fig. 4c**). The rate of dissociation with HflX–GTP ($k_{obs\ HflX–GTP} = 0.4 \pm 0.01\ s^{-1}$) was slower than with RRF, EF-G and IF3 ($k_{obs\ RRF\ +\ EF\text{-}G\ +\ IF3} = 2 \pm 0.03\ s^{-1}$), but the amplitude was the same, thus suggesting that the same level of dissociation had been reached in both cases. Again, HflX showed the highest splitting of the PTL with GMP-PNP (**Fig. 4d**).

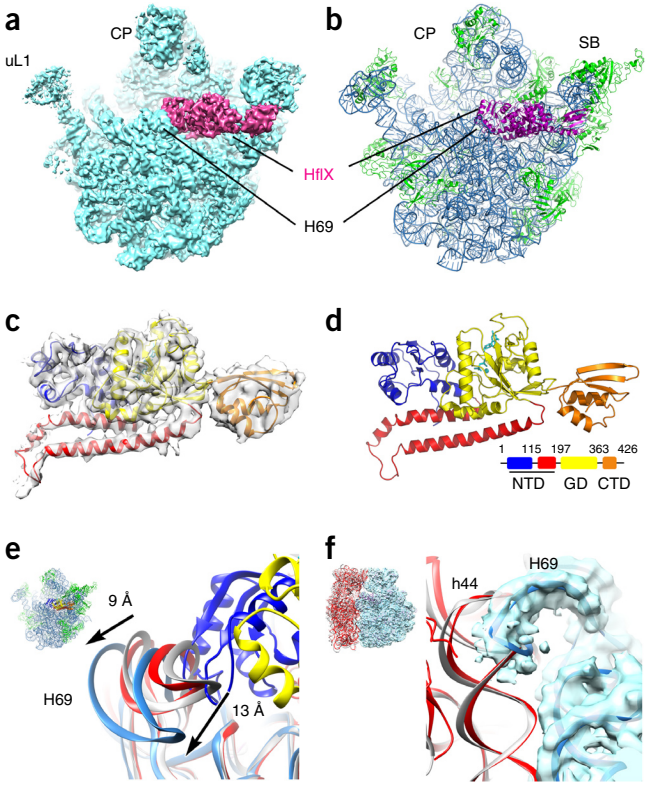

Figure 5 Cryo-EM structure of the 50S–HflX–GMP-PNP complex. (**a**) Surface representation of cryo-EM density map of the 50S–HflX–GMP-PNP complex (4.5 Å), with HflX colored magenta and the 50S subunit colored cyan. (**b**) The atomic model of the 50S–HflX–GMP-PNP complex. The 23S rRNA, ribosomal proteins and HflX are colored marine, green and magenta respectively. (**c**) Segmented density map of HflX (in transparent gray), superimposed with the atomic model of HflX. (**d**) Cartoon representation of the atomic model of the *E. coli* HflX. NTD, N-terminal domain; GD, GTPase domain; CTD, C-terminal domain. The two subdomains of the NTD, subdomain I (residues 1–115) and subdomain II (116–197) are colored blue and red, respectively. (**e**) Local conformational changes of H69 of the 23S rRNA upon HflX binding. The atomic model of the 50S–HflX–GMP-PNP complex (marine) is superimposed with the models of the 50S subunits from crystal structures of two different 70S complexes, an RRF-bound 70S complex (PDB 3R8S, red)[54] and an empty 70S ribosome (PDB 2AWB, gray)[55]. (**f**) Deformed H69 in the 50S–HflX–GMP-PNP complex substantially clashes with h44 in the 30S subunit. The cryo-EM density map (transparent cyan) and the atomic model (marine) of the 50S–HflX–GMP-PNP complex are superimposed with the models of the 30S subunits from the crystal structures of two different 70S complexes, an RRF-bound 70S complex (PDB 4GD1, red)[54] and an empty 70S ribosome (PDB 2AW7, gray)[55].

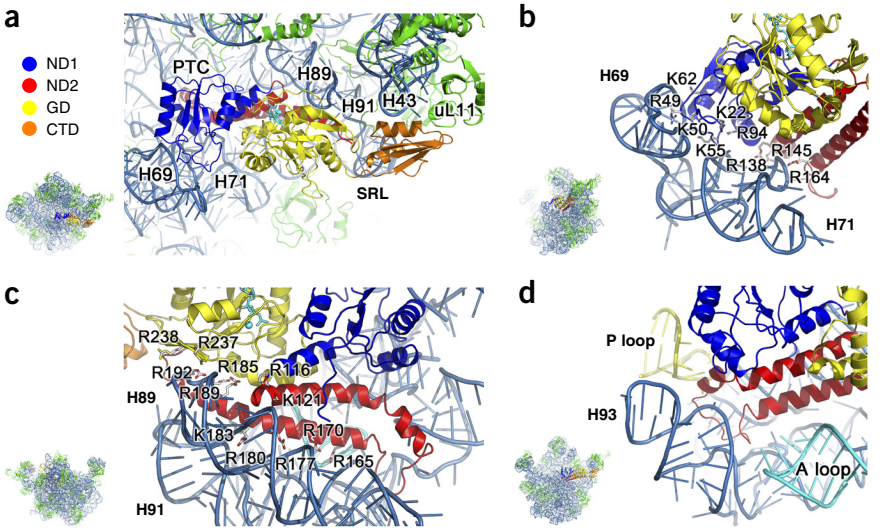

Figure 6 Specific electrostatic interactions between HflX and the 50S subunit. (**a**) Orientation of HflX on the 50S subunit. PTC, peptidyl transferase center; SRL, sarcin-ricin loop. The helices of the 23S rRNA (H69, H71, H89, H91 and H43), which are involved in direct contacts with HflX are labeled. GMP-PNP in the nucleotide-binding pocket is shown in stick model (cyan). (**b**) Atomic interactions between H69-H71 and subdomain I (blue) of the HflX NTD. Basic residues (shown in stick representation) of HflX at the interface are labeled. (**c**) Atomic interactions between H89 and subdomain II (red) of HflX NTD. (**d**) The intervening loop connecting the two α-helices of subdomain II is inserted into the space between the A loop and P loop of the 23S rRNA.

Furthermore, consistently with the polysome breakdown experiments, HflX–GTP was highly inefficient (over 20 min) in splitting ribosomes with a peptidyl tRNA ([^{3}H]fMet-Leu-Ile-tRNA^{Ile}) in the P site (**Fig. 4c**), thus clearly suggesting that deacylation of the P-site tRNA is essential for efficient PTL splitting by HflX.

When we titrated HflX–GTP in increasing concentrations, we observed faster rates and higher extents of splitting of the PTL (**Fig. 4e**). From these titration curves, we determined the binding parameters of HflX–GTP to the PTL (**Fig. 4f**): k_{on} = 0.03 ± 0.0035 $\mu M^{-1}\ s^{-1}$, k_{off} = 0.09 ± 0.01s^{-1}, and K_d = 3 ± 0.01 μM. These values are in the same range as those for the vacant 70S ribosome. Notably, HflX–GTP had a three-fold-higher K_d value for the PTL than for the vacant 70S, thus suggesting that it is easier for HflX to target vacant 70S ribosomes than PTLs.

HflX release from the 50S subunit requires GTP hydrolysis

Because HflX displays preferential binding to the 50S subunit, subunit association might consequentially be affected. Therefore, we followed the kinetics of ribosomal subunit association in the absence and presence of HflX. Indeed, addition of HflX caused slower association of the ribosomal subunits (**Supplementary Fig. 3**). The observed rate of vacant subunit association (4.7 ± 0.1 s^{-1}) decreased to 0.07 ± 0.001s^{-1} in the presence of HflX–GTP (**Supplementary Fig. 3a**). In the case of fully formed 30S preinitiation complex (preIC), the association rate dropped from 22 ± 0.3 s^{-1} without HflX to 0.7 ± 0.03 s^{-1} with HflX–GTP (**Supplementary Fig. 3b**). Interestingly, with the same concentration of HflX–GTP, the rate of 70S formation from 30S preIC (0.7 s^{-1}) was ten-fold higher than from the vacant 30S subunits (0.07 s^{-1}), thus suggesting that HflX is more potent in blocking the formation of vacant 70S. Thus, these results indicate that in addition to its 70S-splitting activity, HflX also preferentially inhibits the association of vacant subunits to form empty 70S ribosomes.

The rate of vacant subunit association in the presence of HflX–GTP (k_{obs} = 0.07 ± 0.001s^{-1}) is comparable to the k_{off} value of HflX (0.05 s^{-1}) estimated from the 70S dissociation experiments (**Fig. 3d**), thus implying that the association of subunits is dependent on and limited by the release of HflX. However, we could not ascertain from either of these experiments whether HflX departs from the ribosome with GTP or GDP. We resolved this ambiguity by conducting subunit association experiments with HflX–GMP-PNP. For both the vacant 30S subunit and 30S preIC, HflX–GMP-PNP completely blocked association of the subunits (**Supplementary Fig. 3a,b**). Thus, GTP hydrolysis on HflX is essential for its release, which is a prerequisite for proper subunit association.

Cryo-EM structure of the 50S subunit bound with HflX–GMP-PNP

The inherent 70S-splitting activity of HflX makes it difficult to study the 70S–HflX complex by structural approaches. Because HflX binds tightly to the 50S subunit, the complex of 50S–HflX–GMP-PNP could presumably represent the state immediately after subunit separation.

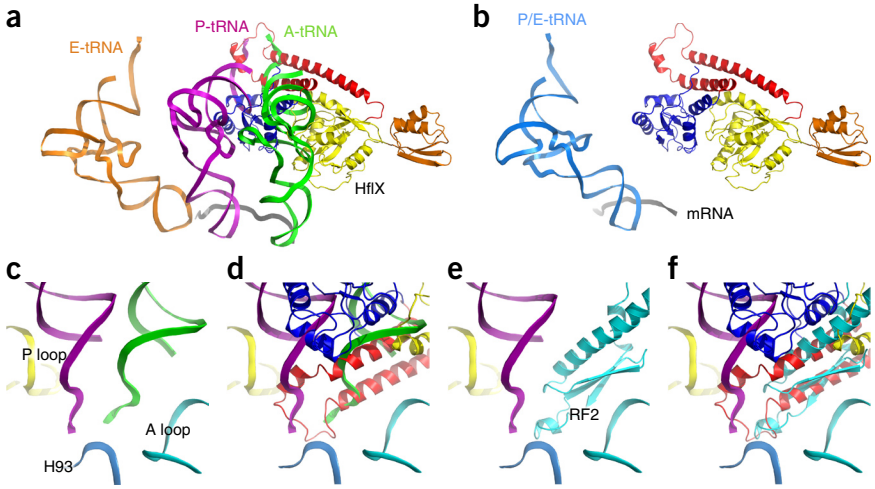

Figure 7 Orientation of HflX relative to tRNAs and release factor 2 on the 50S subunit. (**a**) Superimposition of HflX with A-site tRNA (green) and P-site tRNA (purple) on the ribosome. The coordinates of mRNA (gray) and tRNAs are from a previous work (PDB 2WDK)[56]. A, aminoacyl; P, peptidyl; E, exit. (**b**) Superimposition of HflX with the hybrid P/E-site tRNA (marine) (PDB 4GD1)[54] on the ribosome. (**c**) A zoomed-in view of the ribosomal PTC, in the crystal structure of the three tRNA–containing 70S ribosome (PDB 2WDK)[56]. (**d**) As in **c**, with HflX superimposed. (**e**) A zoomed-in view of the ribosomal PTC, in the crystal structure of the RF2-containing 70S ribosome (PDB 3F1G)[57]. (**f**) As in **e**, with HflX superimposed.

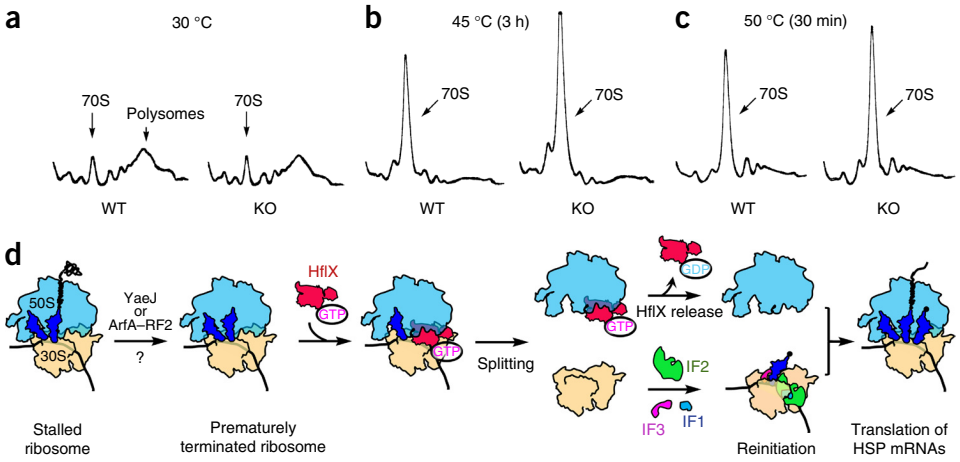

Figure 8 Proposed model for the action of HflX during the heat-shock response. (**a**–**c**) Polysome profile analysis of BW25113 (WT) and Δ*hflX* (KO) cells without (**a**) or with exposure to long, mild (**b**) or short, severe (**c**) heat stress. (**d**) Upon heat shock, elongating ribosomes are paused on mRNAs, which in turn may evoke ribosome-rescuing pathways. The peptides are released from the P-site tRNA by the action of codon-unspecific release factors such as YaeJ and ArfA–RF2, after which the ribosomes undergo ratchet-like movement. HflX–GTP samples ratcheted ribosomes (with hybrid P/E-site tRNA) and splits them into 30S and 50S subunits. Free 30S subunits initiate on HSP mRNAs because of their abundance. Translation on these mRNAs initiates by formation of the 70S initiation complex, after slow release of HflX–GDP from the 50S subunit.

Therefore, to explore the underlying mechanism of ribosome splitting, we applied cryo-EM analysis to the 50S–HflX–GMP-PNP complex. With a flexible fitting approach, we obtained a pseudo-atomic model for the 50S–HflX–GMP-PNP complex from the resulting 4.5-Å cryo-EM density map (**Fig. 5**, **Supplementary Fig. 4a–c** and **Supplementary Movie 1**).

As expected, HflX binds to the intersubunit face of the 50S subunit. While the N-terminal domain (NTD) of HflX protrudes toward the peptidyl transferase center (PTC), making extensive contacts with several rRNA helices (**Fig. 6**), its C-terminal domain (CTD) predominantly interacts with the NTD of uL11 at the bL12 stalk base (**Fig. 6a**). Upon binding to HflX, the 50S subunit undergoes conformational changes mostly in the regions involving intersubunit bridges (**Supplementary Fig. 4d–j**). H69, which forms the major bridge B2a and contacts both A- and P-site tRNAs, shows a massive displacement by 13 Å (**Fig. 5e**). Superimposition of the 50S–HflX–GMP-PNP structure with the 30S subunit showed no direct steric clash between the 30S subunit and HflX. However, the deformed H69 in the 50S–HflX structure substantially overlaps with h44 of the 30S subunit (**Fig. 5f**). This observation explains the strong 70S-splitting activity of HflX and indicates that HflX disrupts bridge B2a in a similar way as RRF does during ribosome recycling[33–35].

Interestingly, when compared with other translation factors, HflX displayed apparent steric clash with almost all of them, with the sole exception of RF3 (**Supplementary Fig. 5a**). Also, although HflX is located at the general binding site of translational GTPases on the 50S subunit, the GTPase domain of HflX is very distinctly oriented on the 50S subunit, so that the nucleotide-binding pocket is away from the sarcin-ricin loop of the 23S rRNA (**Supplementary Fig. 5b**). Therefore, the HflX GTPase activation by the ribosome[17,18] is probably totally different from the activation of the canonical translational GTPases.

The HflX NTD interacts with the PTC

The NTD of HflX can be divided into two subdomains (**Fig. 5d**). Both subdomains have very specific interactions, through surface-exposed basic residues, with the 23S rRNA (**Fig. 6**). There are two electrostatic interfaces between HflX and the 23S rRNA: one involves a large number of basic residues from subdomain I (K22, R49, K50, K55, K62 and R94) and nucleotides from H69 and H71 (**Fig. 6b**); the other is established between subdomain II and H89. Subdomain II is composed of two connecting α-helices, and notably, one helix from subdomain II is oriented in parallel with H89, allowing electrostatic interactions (R165, R170, R177, R180, K183, R185, R189 and R192) from multiple positions on the helix (**Fig. 6c**). Importantly, many of these basic residues on HflX have been highly conserved throughout evolution, thus suggesting that these polar interactions are highly specific.

Intriguingly, the loop connecting the two helices of subdomain II is precisely inserted into the PTC and is situated between the A loop and P loop of the 23S rRNA (**Fig. 6d** and **Supplementary Movie 1**). This loop occupies the position of the CCA end of the A-site tRNA in a strikingly similar fashion to that of the GGQ motif–containing loop of release factors (**Fig. 7**). This observation indicates that, like many translation factors, HflX uses a tRNA-mimicry[36] strategy to interact with the ribosome. Further comparison indicated that the NTD of HflX also overlaps partially with the P-site tRNA but is compatible with the hybrid peptidyl/exit (P/E)-site tRNA (**Fig. 7a**,**b**). This finding could be of physiological importance because it explains why the deacylation of the P-site tRNA is important for efficient ribosome splitting by HflX. The deacylation of the P-site tRNA enables the ribosome to undergo ratchet-like rotational motion[37,38], thus resulting in a hybrid P/E configuration. Therefore, it is highly likely that HflX, as EF-G, RRF and RF3, preferentially samples the rotated conformation when binding to the 70S ribosome.

To validate the structural findings, we introduced two domain truncations (ΔN and ΔC) and several point mutations on subdomains I and II (R49A K50A, K55A K62A, R164A R165A, R168A R170A, R185A R189A and R192A K194A) and tested them in a 70S splitting assay with SDGC. As expected, truncation of either NTD or CTD rendered the protein inactive in 70S splitting (**Supplementary Fig. 6a**). Also unsurprisingly, all point mutations showed a substantial decrease in 70S-splitting activity, and K55A K62A resulted in the lowest activity (nearly zero) of all (**Supplementary Fig. 6b**). The two mutated residues are located at the interface between H69 and subdomain I (**Fig. 6b**). Further validation experiments (**Supplementary Fig. 6c**,**d**) showed that all point mutants bound to the 50S subunit

comparably to WT HflX, thus indicating that these mutations affected the 70S-splitting activity directly rather than affecting the binding of HflX to the 50S subunit.

Collectively, our structural and mutational data suggest that HflX is a new ribosome-dissociating factor. Both the NTD and CTD are required for the 70S-splitting activity, and the NTD is the effector domain.

DISCUSSION

HflX is an alternative ribosome-dissociating factor

Our structural data reveal that the HflX NTD structurally mimics the acceptor arm of the A-site tRNA, displaying a close resemblance to the peptide-release factors (**Fig. 7f**). This finding, together with the structural compatibility between HflX and RF3 on the ribosome (**Supplementary Fig. 5a**), hints that the physiological function of HflX might be related to the termination and recycling of the ribosome. This is further reminiscent of three well-characterized cotranslational surveillance systems in eukaryotes[8], all of which use modified termination and recycling processes to rescue ribosomes trapped in faulty translation. Two termination-like factors in eukaryotes, Dom34 and Hbs1 (homologs of eRF1 and eRF3, respectively), and an eukaryote-specific recycling factor, Rli1, are required to efficiently recycle ribosomes encountering non-stop or no-go mRNAs[39–42] or the poly(A) sequences in the 3′ untranslated regions of regular mRNAs[43] as well as empty ribosomes trapped by the stress factor Stm1 during starvation[44].

During a normal translation cycle, RRF and EF-G catalyze the dissociation of the post-termination complex[45,46]. According to our data, HflX and RRF–EF-G probably constitute two complementary systems in the cell for splitting terminated ribosomes under different physiological conditions. The splitting mediated by RRF–EF-G is dependent on GTP hydrolysis and requires IF3 for stable dissociation. In contrast, HflX splits the PTL without GTP hydrolysis, and the presence of IF3 is not required. In principle, ribosomal substrates for these two systems should be from different upstream events. This is supported by our result that plasmid-based overexpression of RRF in Δ*hflX* cells only partially restored cell growth under high-temperature conditions (**Supplementary Fig. 7**), thus suggesting that the two systems are not redundant. Furthermore, unlike RRF, which cannot efficiently split vacant 70S ribosomes, HflX can complement the IF1-IF3 system[32] for splitting vacant 70S ribosomes. In summary, HflX appears to be a more flexible and economical ribosome-dissociating factor particularly required for cell fitness in heat shock.

Physiological role of HflX during the heat-shock response

Heat shock not only leads to a general repression of translation but also induces pausing of translating ribosomes at early elongation steps[11]. This in turn causes accumulation of nonproductive, stalled ribosomes through various mechanisms[13,14]. Hence, during HSR, cells need to recycle the arrested ribosomal complexes efficiently, mainly to increase the cellular translation capacity. Bacteria possess a well-characterized *trans*-translation system (tmRNA system)[47], which rescues ribosomes stalled on the 3′ ends of non-stop or no-go mRNAs. However, the tight dependence of the tmRNA system on normal elongation and termination processes makes it unlikely to fulfill the need for rapid rescue of the stalled ribosomes, as required during HSR. In addition, bacteria also possess two newly discovered tmRNA-independent rescue pathways, ArfA–RF2 and YaeJ (also known as ArfB) systems (reviewed in ref. 47). However, these two systems are peptidyl-tRNA hydrolase in nature and are not capable of recycling ribosomes.

Our data showing that HflX is a heat shock–induced ribosome-splitting factor makes it a perfect candidate to fulfill cells' urgent need to rescue stalled ribosomes under heat-shock conditions (**Fig. 8**). This hypothesis is supported by our polysome profile analysis of the WT and Δ*hflX* cells. Exposure of the WT and Δ*hflX* cells to heat stress (either a long, mild or a short, severe treatment) led to substantial accumulation of the 70S ribosomes concomitant with the decrease in the polysomes, and the stalling was even more severe in the Δ*hflX* cells. Moreover, after heat treatment, considerably more HflX was in the 50S fractions, and HflX started to accumulate in the polysome fractions (**Supplementary Fig. 8**). According to our data presented in this study, the physiological importance of HflX appears to be two-fold. First, HflX can quickly liberate a large number of ribosomes arrested in nonproductive manners and consequently increase the cellular translation capacity. Second, HflX preferentially blocks association of the vacant 30S subunits with the 50S subunit, as compared to the mRNA-programmed 30S preIC (**Supplementary Fig. 3**). This suggests that the slow departure of HflX from the 50S subunit is physiologically necessary, because it allows enough time for the initiation factors and HSP mRNAs to initiate translation on the 30S subunit and prevents formation of empty 70S ribosomes.

HflX is highly inefficient in splitting a stalled ribosomal complex with peptidyl-tRNA in the P site (**Fig. 4c**), thus suggesting that HflX probably needs to coordinate with additional factors with peptidyl-tRNA hydrolase activity. Such a candidate could be YaeJ[48,49], which catalyzes the hydrolysis of peptidyl-tRNA on the ribosome in a codon-independent manner. Notably, overexpression of YaeJ partially suppresses the temperature-sensitive growth defect of an *E. coli* strain lacking σ^E (Δ*rpoE*)[50], a heat-shock sigma factor that regulates σ^{32} (ref. 51). This fact, together with our observation that HflX is an HSP, further suggests a plausible joint participation of HflX and YaeJ in rescuing stalled ribosomes during HSR (**Fig. 8b**). Phylogenetic evidence that human homologs of both YaeJ (ICT1)[52] and HflX (GTP-binding protein-like, PGPL)[53] localize into the mitochondria further supports this hypothesis.

In conclusion, our results suggest that HflX is an important member of the general translation-rescuing system of the cell, in which noncanonical termination and recycling factors clear nonproductive ribosomes that accumulate in various situations. The functions of these alternative termination and recycling factors are particularly essential in translational reprogramming during the stress response.

METHODS

Methods and any associated references are available in the online version of the paper.

Accession codes. The cryo-EM density map has been deposited in the Electron Microscopy Data Bank under accession number EMD-3133. The fitted atomic model has been deposited in the Protein Data Bank under accession code 5ADY.

Note: Any Supplementary Information and Source Data files are available in the online version of the paper.

ACKNOWLEDGMENTS

This work was funded by grants from the National Natural Science Foundation of China (31170677 and 31422016 to N.G.) and the Ministry of Science and Technology of China (2013CB910404 to N.G.). S.S. acknowledges research funding from the Swedish Research Council (2010-2619 (M), 2011-6088 (NT), 2014-4423 (NT) and 2008-6593 (Linnaeus grant to Uppsala RNA Research Center); and the Knut and Alice Wallenberg Foundation (KAW 2011.0081 to RiboCORE platform)). We thank the National BioResource Project of Japan for providing *E. coli* strains BW25113 and JW4131. We also thank the China National Center for Protein Sciences (Beijing) and Tsinghua National Laboratory for Information Science and Technology ('Explorer 100' cluster system) for providing computational resources.

AUTHOR CONTRIBUTIONS

J.L., S.S. and N.G. designed experiments. Yanqing Zhang performed quantitative PCR, western blotting, cell growth experiments (with X.L. and K.M.), WT and mutant protein preparation (with X.Z.), ribosome purification, SDGC-based experiments, polysome profile analysis (with D.Z. and Y.Q.), cryo-EM data collection (with J.L.) and image processing (with W.C., N.L., Yixiao Zhang and N.G.). C.S.M. performed kinetics experiments. Y.Z., C.S.M., S.S. and N.G. prepared the manuscript; all authors approved the final manuscript.

COMPETING FINANCIAL INTERESTS

The authors declare no competing financial interests.

1. Verghese, J., Abrams, J., Wang, Y. & Morano, K.A. Biology of the heat shock response and protein chaperones: budding yeast (*Saccharomyces cerevisiae*) as a model system. *Microbiol. Mol. Biol. Rev.* **76**, 115–158 (2012).
2. Richter, K., Haslbeck, M. & Buchner, J. The heat shock response: life on the verge of death. *Mol. Cell* **40**, 253–266 (2010).
3. Yura, T., Nagai, H. & Mori, H. Regulation of the heat-shock response in bacteria. *Annu. Rev. Microbiol.* **47**, 321–350 (1993).
4. Lindquist, S. Regulation of protein synthesis during heat shock. *Nature* **293**, 311–314 (1981).
5. Spriggs, K.A., Bushell, M. & Willis, A.E. Translational regulation of gene expression during conditions of cell stress. *Mol. Cell* **40**, 228–237 (2010).
6. Pechmann, S., Willmund, F. & Frydman, J. The ribosome as a hub for protein quality control. *Mol. Cell* **49**, 411–421 (2013).
7. Sherman, M.Y. & Qian, S.B. Less is more: improving proteostasis by translation slow down. *Trends Biochem. Sci.* **38**, 585–591 (2013).
8. Shoemaker, C.J. & Green, R. Translation drives mRNA quality control. *Nat. Struct. Mol. Biol.* **19**, 594–601 (2012).
9. Kramer, G., Boehringer, D., Ban, N. & Bukau, B. The ribosome as a platform for co-translational processing, folding and targeting of newly synthesized proteins. *Nat. Struct. Mol. Biol.* **16**, 589–597 (2009).
10. Hartl, F.U. & Hayer-Hartl, M. Converging concepts of protein folding *in vitro* and *in vivo*. *Nat. Struct. Mol. Biol.* **16**, 574–581 (2009).
11. Shalgi, R. *et al.* Widespread regulation of translation by elongation pausing in heat shock. *Mol. Cell* **49**, 439–452 (2013).
12. Liu, B., Han, Y. & Qian, S.B. Cotranslational response to proteotoxic stress by elongation pausing of ribosomes. *Mol. Cell* **49**, 453–463 (2013).
13. Hayes, C.S. & Sauer, R.T. Cleavage of the A site mRNA codon during ribosome pausing provides a mechanism for translational quality control. *Mol. Cell* **12**, 903–911 (2003).
14. Doma, M.K. & Parker, R. Endonucleolytic cleavage of eukaryotic mRNAs with stalls in translation elongation. *Nature* **440**, 561–564 (2006).
15. Subramaniam, A.R., Zid, B.M. & O'Shea, E.K. An integrated approach reveals regulatory controls on bacterial translation elongation. *Cell* **159**, 1200–1211 (2014).
16. Narberhaus, F. Translational control of bacterial heat shock and virulence genes by temperature-sensing mRNAs. *RNA Biol.* **7**, 84–89 (2010).
17. Jain, N. *et al. E. coli* HflX interacts with 50S ribosomal subunits in presence of nucleotides. *Biochem. Biophys. Res. Commun.* **379**, 201–205 (2009).
18. Shields, M.J., Fischer, J.J. & Wieden, H.J. Toward understanding the function of the universally conserved GTPase HflX from *Escherichia coli*: a kinetic approach. *Biochemistry* **48**, 10793–10802 (2009).
19. Verstraeten, N., Fauvart, M., Versees, W. & Michiels, J. The universally conserved prokaryotic GTPases. *Microbiol. Mol. Biol. Rev.* **75**, 507–542 (2011).
20. Morimoto, T. *et al.* Six GTP-binding proteins of the Era/Obg family are essential for cell growth in *Bacillus subtilis*. *Microbiology* **148**, 3539–3552 (2002).
21. Dutta, D., Bandyopadhyay, K., Datta, A.B., Sardesai, A.A. & Parrack, P. Properties of HflX, an enigmatic protein from *Escherichia coli*. *J. Bacteriol.* **191**, 2307–2314 (2009).
22. Gerdes, S.Y. *et al.* Experimental determination and system level analysis of essential genes in *Escherichia coli* MG1655. *J. Bacteriol.* **185**, 5673–5684 (2003).
23. Engels, S. *et al.* The transcriptional activator ClgR controls transcription of genes involved in proteolysis and DNA repair in *Corynebacterium glutamicum*. *Mol. Microbiol.* **57**, 576–591 (2005).
24. Chuang, S.E. & Blattner, F.R. Characterization of twenty-six new heat shock genes of *Escherichia coli*. *J. Bacteriol.* **175**, 5242–5252 (1993).
25. Richmond, C.S., Glasner, J.D., Mau, R., Jin, H. & Blattner, F.R. Genome-wide expression profiling in *Escherichia coli* K-12. *Nucleic Acids Res.* **27**, 3821–3835 (1999).
26. Carruthers, M.D. & Minion, C. Transcriptome analysis of *Escherichia coli* O157:H7 EDL933 during heat shock. *FEMS Microbiol. Lett.* **295**, 96–102 (2009).
27. Fischer, J.J. *et al.* The ribosome modulates the structural dynamics of the conserved GTPase HflX and triggers tight nucleotide binding. *Biochimie* **94**, 1647–1659 (2012).
28. Blombach, F. *et al.* An HflX-type GTPase from *Sulfolobus solfataricus* binds to the 50S ribosomal subunit in all nucleotide-bound states. *J. Bacteriol.* **193**, 2861–2867 (2011).
29. Polkinghorne, A. *et al. Chlamydophila pneumoniae* HflX belongs to an uncharacterized family of conserved GTPases and associates with the *Escherichia coli* 50S large ribosomal subunit. *Microbiology* **154**, 3537–3546 (2008).
30. Antoun, A., Pavlov, M.Y., Tenson, T. & Ehrenberg, M.M. Ribosome formation from subunits studied by stopped-flow and Rayleigh light scattering. *Biol. Proced. Online* **6**, 35–54 (2004).
31. Wilson, D.N. The A-Z of bacterial translation inhibitors. *Crit. Rev. Biochem. Mol. Biol.* **44**, 393–433 (2009).
32. Pavlov, M.Y., Antoun, A., Lovmar, M. & Ehrenberg, M. Complementary roles of initiation factor 1 and ribosome recycling factor in 70S ribosome splitting. *EMBO J.* **27**, 1706–1717 (2008).
33. Gao, N. *et al.* Mechanism for the disassembly of the posttermination complex inferred from cryo-EM studies. *Mol. Cell* **18**, 663–674 (2005).
34. Weixlbaumer, A. *et al.* Crystal structure of the ribosome recycling factor bound to the ribosome. *Nat. Struct. Mol. Biol.* **14**, 733–737 (2007).
35. Borovinskaya, M.A. *et al.* Structural basis for aminoglycoside inhibition of bacterial ribosome recycling. *Nat. Struct. Mol. Biol.* **14**, 727–732 (2007).
36. Nakamura, Y. & Ito, K. tRNA mimicry in translation termination and beyond. *Wiley Interdiscip. Rev. RNA* **2**, 647–668 (2011).
37. Valle, M. *et al.* Locking and unlocking of ribosomal motions. *Cell* **114**, 123–134 (2003).
38. Frank, J. & Agrawal, R.K. A ratchet-like inter-subunit reorganization of the ribosome during translocation. *Nature* **406**, 318–322 (2000).
39. Shoemaker, C.J. & Green, R. Kinetic analysis reveals the ordered coupling of translation termination and ribosome recycling in yeast. *Proc. Natl. Acad. Sci. USA* **108**, E1392–E1398 (2011).
40. Pisareva, V.P., Skabkin, M.A., Hellen, C.U., Pestova, T.V. & Pisarev, A.V. Dissociation by Pelota, Hbs1 and ABCE1 of mammalian vacant 80S ribosomes and stalled elongation complexes. *EMBO J.* **30**, 1804–1817 (2011).
41. Shoemaker, C.J., Eyler, D.E. & Green, R. Dom34:Hbs1 promotes subunit dissociation and peptidyl-tRNA drop-off to initiate no-go decay. *Science* **330**, 369–372 (2010).
42. Tsuboi, T. *et al.* Dom34:hbs1 plays a general role in quality-control systems by dissociation of a stalled ribosome at the 3′ end of aberrant mRNA. *Mol. Cell* **46**, 518–529 (2012).
43. Guydosh, N.R. & Green, R. Dom34 rescues ribosomes in 3′ untranslated regions. *Cell* **156**, 950–962 (2014).
44. van den Elzen, A.M., Schuller, A., Green, R. & Seraphin, B. Dom34-Hbs1 mediated dissociation of inactive 80S ribosomes promotes restart of translation after stress. *EMBO J.* **33**, 265–276 (2014).
45. Zavialov, A.V., Hauryliuk, V.V. & Ehrenberg, M. Splitting of the posttermination ribosome into subunits by the concerted action of RRF and EF-G. *Mol. Cell* **18**, 675–686 (2005).
46. Hirokawa, G. *et al.* Post-termination complex disassembly by ribosome recycling factor, a functional tRNA mimic. *EMBO J.* **21**, 2272–2281 (2002).
47. Shimizu, Y. Biochemical aspects of bacterial strategies for handling the incomplete translation processes. *Front. Microbiol.* **5**, 170 (2014).
48. Chadani, Y., Ono, K., Kutsukake, K. & Abo, T. *Escherichia coli* YaeJ protein mediates a novel ribosome-rescue pathway distinct from SsrA- and ArfA-mediated pathways. *Mol. Microbiol.* **80**, 772–785 (2011).
49. Handa, Y., Inaho, N. & Nameki, N. YaeJ is a novel ribosome-associated protein in *Escherichia coli* that can hydrolyze peptidyl-tRNA on stalled ribosomes. *Nucleic Acids Res.* **39**, 1739–1748 (2011).
50. Connolly, L., De Las Penas, A., Alba, B.M. & Gross, C.A. The response to extracytoplasmic stress in *Escherichia coli* is controlled by partially overlapping pathways. *Genes Dev.* **11**, 2012–2021 (1997).
51. Wang, Q.P. & Kaguni, J.M. A novel sigma factor is involved in expression of the rpoH gene of *Escherichia coli*. *J. Bacteriol.* **171**, 4248–4253 (1989).
52. Wesolowska, M.T., Richter-Dennerlein, R., Lightowlers, R.N. & Chrzanowska-Lightowlers, Z.M. Overcoming stalled translation in human mitochondria. *Front. Microbiol.* **5**, 374 (2014).
53. Gianfrancesco, F. *et al.* A novel pseudoautosomal gene encoding a putative GTP-binding protein resides in the vicinity of the Xp/Yp telomere. *Hum. Mol. Genet.* **7**, 407–414 (1998).
54. Dunkle, J.A. *et al.* Structures of the bacterial ribosome in classical and hybrid states of tRNA binding. *Science* **332**, 981–984 (2011).
55. Schuwirth, B.S. *et al.* Structures of the bacterial ribosome at 3.5 A resolution. *Science* **310**, 827–834 (2005).
56. Voorhees, R.M., Weixlbaumer, A., Loakes, D., Kelley, A.C. & Ramakrishnan, V. Insights into substrate stabilization from snapshots of the peptidyl transferase center of the intact 70S ribosome. *Nat. Struct. Mol. Biol.* **16**, 528–533 (2009).
57. Korostelev, A. *et al.* Crystal structure of a translation termination complex formed with release factor RF2. *Proc. Natl. Acad. Sci. USA* **105**, 19684–19689 (2008).

ONLINE METHODS

Plasmid construction. Polymerase chain reaction (PCR) was conducted to amplify the *hflX* gene (from *E. coli* DH5α) with primers listed in **Supplementary Table 1**. The amplified DNA fragment was cloned into the pET28a, pProEX and pBAD plasmids by double digestion with enzymes (NdeI and XhoI for pET28a, and NcoI and XhoI for pProEX and pBAD); this was followed by ligation with standard methods. Constructions for mutations and truncations of HflX protein were carried out with pProEx plasmid with the primers listed in **Supplementary Table 1**. The gene for RRF was also cloned into the pBAD vector (pBAD-frr) with the same strategy.

Protein purification. The pET28a-hflX plasmid was transformed into *E. coli* BL21(DE3) cells for protein expression. Cells in mid-log phase were induced with 1 mM isopropyl-β-D-thiogalactopyranoside (IPTG) (Sigma-Aldrich) for 15 h at 16 °C. Cells were harvested and lysed in buffer A (20 mM Tris-HCl, pH 8.0, 500 mM NaCl, and 20 mM imidazole) by ultrasonication. After centrifugation of cell lysates, supernatants were loaded onto a HisTrap HP Ni-NTA column (GE Healthcare) and eluted with buffer B (20 mM Tris-HCl, pH 8.0, 500 mM NaCl, and 500 mM imidazole). Fractions containing HflX were pooled, concentrated, and applied onto a gel-filtration column of Superdex 75 10/300GL (GE Healthcare) preequilibrated with buffer C (20 mM Tris-HCl, pH 8.0, 500 mM NaCl, and 2 mM dithiothreitol (DTT)). HflX proteins were divided into aliquots, flash frozen with liquid nitrogen, and stored at −80 °C for further use. The purification for mutated and truncated variants of HflX was carried out similarly as described above, with an additional step of TEV enzyme digestion to remove the histidine tag before gel filtration (Superdex 75 10/300GL, GE Healthcare).

RT-qPCR. The experiments were performed according to a published protocol[58]. 500-μl aliquots of *E. coli* BW25113 cells in mid-log phase were further incubated at either 30 °C or 50 °C for different time ranges (2, 4, 6, 8, 10, 15 or 20 min). Total RNA was purified with a GeneJET RNA purification kit (Thermo Scientific). The cDNAs were synthesized by a reverse-transcription kit (TOYOBO), and quantified with a quantitative PCR system (Agilent Technologies) with primers listed in **Supplementary Table 1**. Each measurement was repeated three times. Results were analyzed with MxPro QPCR software. The 16S rRNA was used as the internal control, and *dnaK* and *rpoA* were the positive and negative controls, respectively.

Western blotting. *E. coli* BW25113 cells were cultured in 100 ml LB medium at 30 °C to an OD_{600} of ~0.2 and split into 1-ml aliquots in Eppendorf tubes. Each tube was incubated at either 45 °C or 30 °C in water. Cells were harvested at different time points (10, 20, 30, 40, 50 or 60 min), by centrifugation at 13,000 r.p.m. for 30 s at room temperature, and flash frozen in liquid nitrogen. Pellets were resolved in a buffer containing 10 mM Tris-HCl, pH 6.8, 8 M urea, 0.4% (w/v) SDS, 10% (v/v) glycerol, 5 mM DTT, and 1 mM PMSF. 0.2 A_{260} units of samples were loaded onto a SDS-PAGE gel and analyzed by western blotting with a semidry transfer cell (Trans-Blot SD, Bio-Rad). Primary anti-HflX was prepared by injection of full-length recombinant HflX protein into rabbits and was purified with the C-terminal domain of HflX via affinity chromatography, through a customized service (CW Biotech, Beijing). Antibodies specific to DnaK (Abcam, ab69617) and RNA polymerase α subunit (Santa Cruz Biotechnology, sc-101597) were from commercial sources. Verification of these three primary antibodies is provided in the **Supplementary Note**.

Spotting assay and determination of colony-forming units (CFUs). *Long, mild heat stress.* Early-log-phase cultures (LB, 30 °C) of *E. coli* cells of BW25113 (WT) or JW4131 (Δ*hflX*) strains were diluted to an OD_{600} of 0.1 and subjected to five ten-fold serial dilutions. 4 μl of each dilution was spotted on LB plates and incubated for 18 h at 45 °C or 30 °C. For CFU/ml determination, aliquots (50 μl) of serially diluted (1:10) cultures were spread onto LB plates. The plates were incubated at 45 °C or 30 °C, and values of CFU/ml were determined after 1-d incubation. Three parallel experiments were carried out.

Short, severe heat stress. 100-μl aliquots of early-log-phase cells (BW25113 or JW4131) grown as above, were further transferred to 50 °C or 30 °C for 30 min, and subjected to five ten-fold serial dilutions. 4 μl of each dilution was spotted onto LB plates, and this was followed by incubation at 30 °C for 18 h. The determination of CFU/mL was carried out similarly, as described above.

Growth-curve measurements. Overnight cultures (LB, 30 °C) of BW25113 and JW4131 strains were diluted 1,000-fold in LB medium. 200-μl aliquots of the diluted culture were transferred to a 96-well plate. The OD_{600} was recorded every 30 min in a programmable plate reader (Thermo Scientific, Varioskan Flash) with continuous shaking at 30 °C or 45 °C. The growth curves were constructed by averaging three parallel experiments.

Genetic complementation. Early-log-phase cultures (OD_{600} of ~0.2) of WT-pBAD, ΔhflX-pBAD, ΔhflX-pBADfrr and ΔhflX-pBADhflX strains were diluted to OD_{600} of 0.1 and grown at 50 °C or 30 °C for the indicated time in LB medium containing 50 μg/ml ampicillin and 0.2% L-arabinose. Spotting assays and CFU determination (**Supplementary Fig. 7**) were carried out as described above.

Immunodetection of endogenous HflX distribution in cellular sedimentation fractions. Cell lysate was prepared with a standard freeze-thaw method[59]. Mid-log-phase cultures of *E. coli* BW25113 strain grown at the indicated temperatures (30 °C or 45 °C) were treated with chloramphenicol (final concentration, 200 μg/ml) and harvested after 3 min. Cultures were then poured onto chipped ice with the same volume and centrifuged at 8,000 r.p.m. for 3 min at 4 °C. Cell pellets were resuspended in 1 ml cold lysis buffer containing 20 mM Tris-HCl, pH 7.5, 100 mM NH_4Cl, 10 mM $Mg(OAc)_2$, 4 mM β-mercaptoethanol, 1 mg/ml lysozyme, 100 U/ml RNase-free DNase I (New England BioLabs), 0.5 U/μl recombinant RNase inhibitor (TaKaRa), and 0.3% (w/v) deoxycholate (DOC) (Sigma-Aldrich), flash frozen with liquid nitrogen and thawed in an ice-water bath. The freeze-thaw cycles were repeated three times. Lysates were cleared by centrifugation at 13,000 r.p.m. for 30 min at 4 °C. Eight A_{260} units of clarified lysate was loaded onto a 10%-to-50% (w/v) sucrose gradient in buffer I (20 mM Tris-HCl, pH 7.5, 100 mM NH_4Cl, and 10 mM $Mg(OAc)_2$) with 4 mM β-mercaptoethanol and centrifuged at 36,000 r.p.m. for 3.5 h at 4 °C with a SW41 rotor (Beckman Coulter). Gradients were analyzed by passage through a UV monitor, and fixed-volume fractions were collected with a density gradient fractionator (Teledyne Isco). HflX was detected after TCA precipitation of the fractions and subsequent western blotting, as described above.

Cosedimentation assay. *E. coli* ribosomes and the ribosomal subunits were obtained as previously described[60]. 0.3 μM 50S subunits were mixed with 0.9 μM HflX (wild type or various mutants) in 100 μl buffer I, in the presence of GMP-PNP (final concentration 1 mM), and the reaction mixtures were incubated at 37 °C for 15 min. 90 μl of mixtures was loaded onto a 33% (w/v) sucrose cushion (prepared with buffer I) and centrifuged at 95,000 r.p.m. for 2.5 h at 4 °C with a TLA-100 rotor (Beckman Coulter). Supernatants were rapidly removed, and pellets were resuspended in buffer I and analyzed by 15% SDS-PAGE. As a control, identical procedures were performed with wild-type or mutant forms of HflX alone, and both supernatants (processed with TCA precipitation) and pellets were examined by SDS-PAGE.

HflX binding assay with sucrose density gradient centrifugation (SDGC). Each reaction (200 μl in buffer I) contained HflX (1.8 μM), purified ribosomes or ribosomal subunits (70S, 30S, and 50S, 0.6 μM), and 1 mM GMP-PNP/GTP/GDP. Reaction mixtures were incubated at 37 °C for 15 min, loaded onto a 10%-to-40% (w/v) sucrose density gradient (prepared in buffer I), and centrifuged at 39,000 r.p.m. for 3.5 h at 4 °C with a SW41 rotor (Beckman Coulter). Pellets were analyzed with 15% SDS-PAGE after gradient fractionation and TCA precipitation.

Equilibrium 70S ribosome splitting assay. Each reaction (200 μl) contained purified 70S ribosome (0.3 μM) and 20-fold excess of HflX, with different nucleotides (GMP-PNP/GTP/GDP/apo, final concentration 1 mM) in buffer I. Mixtures were incubated at 37 °C for 15 min and centrifuged with SDGC as described above. Similarly to procedures for purified 70S ribosomes, the splitting assay was performed with cell lysate derived from ultrasonication (**Supplementary Fig. 2**).

Polysome breakdown assay. Polysomes were prepared by a previously described method[61] with minor modifications. Mid-log-phase *E. coli* BW25113 cells incubated at 37 °C were treated with 0.3 mM tetracycline (Sigma-Aldrich) for 3 min; this was followed by repeated freeze-thaw as described above. Supernatant of the lysate, derived by centrifugation at 13,000 r.p.m. for 30 min at 4 °C, was loaded onto a 10%-to-50% (w/v) sucrose gradient in buffer I and further centrifuged

at 30,000 r.p.m. for 3.5 h at 4 °C in a SW32 rotor (Beckman Coulter). Gradients were collected as described above, and fractions containing polysomes (2× and heavier) were pooled and stored at −80 °C for further use. Splitting of polysomes by HflX was assayed in a similar way as previously described for EF-G and RRF[62]. Each reaction mixture (100 µl) contained fixed amounts of HflX (5 µM), nucleotide (GMP-PNP or GTP, 0.5 mM), and polysome (0.1 µM) without or with the pretreatment of puromycin (0.2 mM) (Sigma-Aldrich) in buffer I (with 4 mM β-mercaptoethanol). Mixtures were incubated at 30 °C for 45 min, loaded onto a 10%-to-40% (w/v) sucrose gradient and centrifuged at 36,000 r.p.m. in a SW41 rotor at 4 °C for 3 h. The gradients were similarly analyzed as described above. Splitting assays of control experiments with or without puromycin were carried out with a reaction system containing 0.3 µM 70S ribosome, 0.45 µM HflX, and 1 mM GMP-PNP or GTP in 100 µl buffer I.

HflX-overexpression experiments. *E. coli* BW25113 cells were transformed with pBAD-hflX plasmid or empty pBAD plasmid.

Growth curves. Overnight cultures derived from a single colony were diluted to an OD_{600} of 0.1 in 100 ml LB medium containing 1% (w/v) L-arabinose and incubated at 37 °C. The OD_{600} values of cultures were recorded once per 30 min until stationary phase was reached.

Ribosome profile analysis. 100 µl of overnight culture was inoculated into 100 ml fresh LB medium without or with 1% or 2% (w/v) L-arabinose (Sigma-Aldrich) at 37 °C. The processes of cell harvest, freeze-thaw lysis, sucrose density gradient centrifugation, and western blotting were carried out similarly as described above. Anti–histidine tag mouse monocolonal antibody (CWBio, CW0082A) was used to examine the expression level of HflX induced by L-arabinose.

Polysome profile analysis of WT and KO cells upon heat shock. Polysome profile analysis (**Fig. 8a**) was carried out as described above. Specifically, WT (BW25113) and KO (Δ*hflX*) cells were cultivated at 30 °C to an OD_{600} of ~0.6 and collected for polysome profile analysis. For the long, mild heat treatment, WT and KO cells were cultivated at 45 °C for 3 h (OD_{600} of ~0.6) and collected for polysome profile analysis. For the short, severe heat treatment, WT and KO cells were first cultivated at 30 °C for 3 h, transferred to 50 °C for 30 min (OD_{600} of ~0.6) and collected for polysome profile analysis. The loading of cell lysates was normalized by values of A_{260} (5 A_{260} units were loaded to top of sucrose gradient).

Pre–steady state kinetics experiments. All translation components used in the kinetics experiments (70S ribosome, 30S and 50S subunits, XR7 mRNA coding Met-Leu-Ile stop (UAA), [^{3}H]fMet-tRNA^{fMet}, tRNA^{Leu}, translation factors RRF, EF-G, IF1, IF2, and IF3) were from *E. coli* and were purified to homogeneity as previously described[63,64]. All pre–steady state kinetics experiments were conducted at 37 °C in HEPES-polymix buffer, pH 7.5 (ref. 64), in the presence of an energy pump containing 1 mM each of ATP and GXP (GTP/GMP-PNP/GDP), PEP (10 mM), pyruvate kinase (50 µg/ml), and myokinase (2 µg/ml) as described in ref. 65. The PTL was produced by incubating 70S ribosomes (0.5 µM) with XR7-fMet-Leu-Ile-stop mRNA (1 µM) and uncharged tRNA^{Leu} (1 µM) at 37 °C for 5 min. The translating ribosomal complex with peptidyl-tRNA in the P site was produced by mixture of 70S ribosomes (0.5 µM) with XR7-fMet-Leu-Ile-stop mRNA (1 µM), [^{3}H]fMet-tRNA^{fMet} (1 µM), IF1, IF2, IF3, EF-Tu, EF-Ts, and EF-G (all 1–2 µM), bulk tRNA from *E. coli*, amino acids leucine and isoleucine. The reaction mix was incubated at 37 °C for 5 min, and the occupancy of [^{3}H]fMet-Leu-Ile-tRNA^{Ile} in the P site was confirmed by checking the peptide in HPLC.

Kinetics of dissociation of vacant 70S ribosome and PTL. Two reaction mixes were prepared in HEPES polymix buffer, pH 7.5. Mix A contained either 70S ribosomes or PTLs or translating ribosomes with [^{3}H]fMet-Leu-Ile-tRNA^{Ile} in the P site (all 0.5 µM), according to a protocol reported previously[32]. Mix B contained different combinations of ribosome-recycling factors such as RRF (20 µM) and EF-G (10 µM) and IF3 (2 µM); IF1 (2 µM) and IF3 (2 µM); or HflX (0-20 µM). Equal volumes of the two reaction mixtures were mixed rapidly in the stopped-flow instrument at 37 °C so that the final concentrations were half of the initial concentrations in the reaction mix. The dissociation of the vacant 70S or PTL into the subunits was monitored by following the decrease in Rayleigh light scattering at 365 nm, with a 320-nm-cutoff filter. Each experiment was done in at least triplicate, and the rates (k_{obs}) were derived by fitting the raw data points with exponential model in Origin 8.0. The HflX-mediated dissociations were performed in the presence of GTP unless otherwise specified. Estimation of dissociation constants from titration data was performed as previously described in ref. 66.

Kinetics of subunit association. Two mixtures A and B were made in polymix, Mix A contained 30S (0.5 µM) alone (naked subunit) or 30S pre-IC containing 30S (0.5 µM) along with IF1 (2 µM), IF2 (2.5 µM), XR7 mRNA coding for MLI (2 µM), fMet-tRNA^{fMet} (2 µM), and GTP 100 µM (30S preIC). Mix B contained either 50S (0.5 µM) alone or together with 2 µM of apo-HflX or HflX–GXP (GTP or GMP-PNP). Both the mixtures were incubated at 37 °C for 5 min, and equal volumes were rapidly mixed in the stopped-flow instrument. The extent of 70S formation was monitored by Rayleigh light scattering at a 365-nm wavelength with a 320-nm-cutoff filter[64], and the observed rates (k_{obs}) were derived by fitting the data with the model previously described by Antoun *et al.*[30].

Cryo-EM sample preparation, data collection and image processing. The 50S–HflX–GMP-PNP complex was formed by incubation of purified components in buffer I at 37 °C for 20 min. The reaction solution (100 µl) contained 50 nM 50S subunit, 1 µM HflX and 1 mM GMP-PNP. A 4-µl aliquot of reaction solution was loaded on a carbon-coated Quantifoil 2/4 grid (Quantifoil Micro Tools), and the cryo-grid was prepared with an FEI Vitrobot (Mark IV). Micrographs were recorded with a Titan Krios (FEI) microscope operated at 300 kV under low-dose conditions with an FEI eagle 4,000 × 4,000 CCD camera. The nominal magnification was 75,000. A total of 9,564 micrographs were collected with AutoEMation automated data collection software[67]. Micrograph screening (6,022 kept) and initial particle picking (903,634 in total) were performed with the SPIDER package[68]. Particles were first picked with a method based on a locally normalized cross-correlation function[69], subjected to correspondence analysis and then manually verified[70]. A final number of 384,206 particles (decimated by a factor of two) were subjected to 3D classification with RELION (version 1.3)[71]. The particles were split into five groups; however, no meaningful difference between class volumes was seen. As a result, all the particles (full size with effective pixel size of 1.166 Å) were combined and subjected to structural refinement with RELION, which rendered a density map at 4.5-Å resolution (gold standard Fourier shell correlation r0.143 criteria) (**Supplementary Fig. 4a–c**). The local resolution map was constructed with ResMap[72].

Modeling and flexible fitting. The atomic model of *E. coli* HflX was modeled from the crystal structure of *Sulfolobus solfataricus* HflX (PDB 3KXI)[73]. The homology modeling was performed with MODELLER[74]. The model of the CTD of *E. coli* HflX was independently modeled by I-TASSER[75] (template PDB 2WBM, residues 164–232)[76]. The switch I region disordered in the crystal structure of *S. solfataricus* HflX was modeled with the crystal structure of *S. thermophilus* NFeoB (PDB 3B1X)[77] as a template. GMP-PNP was derived from a previous model (PDB 3B1X) and docked into the atomic model of the *E. coli* HflX. Atomic models of HflX and the 50S subunit (PDB 3FIK)[78] were docked into the cryo-EM density map with the method of molecular dynamics flexible fitting[79]. Chimera[80] and PyMOL (http://pymol.org/) were used for structural analysis and figure preparation.

58. Schmittgen, T.D. & Livak, K.J. Analyzing real-time PCR data by the comparative C(T) method. *Nat. Protoc.* **3**, 1101–1108 (2008).
59. Ron, E.Z., Kohler, R.E. & Davis, B.D. Polysomes extracted from *Escherichia coli* by freeze-thaw-lysozyme lysis. *Science* **153**, 1119–1120 (1966).
60. Feng, B. *et al.* Structural and functional insights into the mode of action of a universally conserved Obg GTPase. *PLoS Biol.* **12**, e1001866 (2014).
61. Rao, A.R. & Varshney, U. Specific interaction between the ribosome recycling factor and the elongation factor G from *Mycobacterium tuberculosis* mediates peptidyl-tRNA release and ribosome recycling in *Escherichia coli*. *EMBO J.* **20**, 2977–2986 (2001).
62. Hirashima, A. & Kaji, A. Role of elongation factor G and a protein factor on the release of ribosomes from messenger ribonucleic acid. *J. Biol. Chem.* **248**, 7580–7587 (1973).
63. Huang, C., Mandava, C.S. & Sanyal, S. The ribosomal stalk plays a key role in IF2-mediated association of the ribosomal subunits. *J. Mol. Biol.* **399**, 145–153 (2010).
64. Mandava, C.S. *et al.* Bacterial ribosome requires multiple L12 dimers for efficient initiation and elongation of protein synthesis involving IF2 and EF-G. *Nucleic Acids Res.* **40**, 2054–2064 (2012).

doi:10.1038/nsmb.3103

65. Koripella, R.K. *et al.* Mechanism of elongation factor-G-mediated fusidic acid resistance and fitness compensation in *staphylococcus aureus*. *J. Biol. Chem.* **287**, 30257–30267 (2012).
66. Goodrich, J.A. & Kugel, J.F. *Binding and Kinetics for Molecular Biologists* (CSHL press, New York, 2007).
67. Lei, J. & Frank, J. Automated acquisition of cryo-electron micrographs for single particle reconstruction on an FEI Tecnai electron microscope. *J. Struct. Biol.* **150**, 69–80 (2005).
68. Shaikh, T.R. *et al.* SPIDER image processing for single-particle reconstruction of biological macromolecules from electron micrographs. *Nat. Protoc.* **3**, 1941–1974 (2008).
69. Rath, B.K. & Frank, J. Fast automatic particle picking from cryo-electron micrographs using a locally normalized cross-correlation function: a case study. *J. Struct. Biol.* **145**, 84–90 (2004).
70. Shaikh, T.R., Trujillo, R., LeBarron, J.S., Baxter, W.T. & Frank, J. Particle-verification for single-particle, reference-based reconstruction using multivariate data analysis and classification. *J. Struct. Biol.* **164**, 41–48 (2008).
71. Scheres, S.H. A Bayesian view on cryo-EM structure determination. *J. Mol. Biol.* **415**, 406–418 (2012).
72. Kucukelbir, A., Sigworth, F.J. & Tagare, H.D. Quantifying the local resolution of cryo-EM density maps. *Nat. Methods* **11**, 63–65 (2014).
73. Huang, B. *et al.* Functional study on GTP hydrolysis by the GTP-binding protein from *Sulfolobus solfataricus*, a member of the HflX family. *J. Biochem.* **148**, 103–113 (2010).
74. Sali, A. & Blundell, T.L. Comparative protein modelling by satisfaction of spatial restraints. *J. Mol. Biol.* **234**, 779–815 (1993).
75. Roy, A., Kucukural, A. & Zhang, Y. I-TASSER: a unified platform for automated protein structure and function prediction. *Nat. Protoc.* **5**, 725–738 (2010).
76. Ng, C.L. *et al.* Conformational flexibility and molecular interactions of an archaeal homologue of the Shwachman-Bodian-Diamond syndrome protein. *BMC Struct. Biol.* **9**, 32 (2009).
77. Ash, M.R., Maher, M.J., Guss, J.M. & Jormakka, M. A suite of Switch I and Switch II mutant structures from the G-protein domain of FeoB. *Acta Crystallogr. D Biol. Crystallogr.* **67**, 973–980 (2011).
78. Villa, E. *et al.* Ribosome-induced changes in elongation factor Tu conformation control GTP hydrolysis. *Proc. Natl. Acad. Sci. USA* **106**, 1063–1068 (2009).
79. Trabuco, L.G., Villa, E., Mitra, K., Frank, J. & Schulten, K. Flexible fitting of atomic structures into electron microscopy maps using molecular dynamics. *Structure* **16**, 673–683 (2008).
80. Pettersen, E.F. *et al.* UCSF Chimera: a visualization system for exploratory research and analysis. *J. Comput. Chem.* **25**, 1605–1612 (2004).